Theoretical Study on the Reaction of Ti^+ with Acetone and the Role of Intersystem Crossing

Joonghan Kim,[†] Tae Kyu Kim,[‡,*] and Hyotcherl Ihee[†,*]

Center for Time-Resolved Diffraction, Department of Chemistry, Graduate School of Nanoscience & Technology (WCU), KAIST, Daejeon, 305-701, Republic of Korea, and Department of Chemistry and Chemistry Institute for Functional Materials, Pusan National University, Busan, 609-735, Republic of Korea

Received: June 2, 2009; Revised Manuscript Received: September 5, 2009

Ti^+ is known to react with acetone (CH_3COCH_3) to produce TiO^+ and CH_2CHCH_3 as products, but the detailed reaction mechanism and the most favorable reaction pathway have not yet been elucidated. Here, we investigate the doublet and quartet potential-energy surfaces associated with the gas-phase reaction between Ti^+ and acetone for three plausible pathways, (i) direct metal-ion insertion into the C═O bond, (ii) direct H shift, and (iii) metal-mediated H migration, by using the density functional theory (DFT) and ab initio methods. The molecular structures of intermediates and transition states involved in these reaction pathways are optimized at the DFT level by using the PBE0 functional. All transition states are identified by using the intrinsic reaction coordinate (IRC) method, and the resulting reaction coordinates describe how Ti^+ activates the C═O bond of CH_3COCH_3 (acetone) and yields TiO^+ and CH_2CHCH_3 (propene) as products. The intersystem crossing (ISC) point is optimized by a multireference ab initio method, and spin-orbit effects are considered around the ISC point. On the basis of the presented results, we propose that the most favorable reaction pathway proceeds via the direct metal-ion insertion into the C═O bond and passes through an ISC point.

Introduction

Selective activation of chemical bonds such as C−C, C−H, and C═O plays an important role in optimizing economical synthetic routes in organic chemistry.[1] Such activation generally does not occur spontaneously but instead needs to be assisted by suitable catalysts. Understanding the chemical reactions of a transition-metal ion with an organic molecule in the gas phase may provide useful insights for designing better catalysts.[2−4] For this reason, there have been many theoretical investigations aiming at explaining the reaction mechanisms of the first-row transition-metal ions with organic molecules (acetaldehyde,[5−8] ethane,[9] propane,[10] ethylene,[11,12] acetylene,[13] dimethyl ether,[14,15] acetone,[16] allylamine,[17] methyl nitrate,[18] ethyl amine,[19] ethylenediamine,[20] and methanol[21]). In particular, the reactions of metal cations with acetaldehyde have been extensively studied, and each reaction pathway appears to vary depending on the metal ion involved.[5−8] Early transition-metal cations such as Ti^+ and Sc^+ exhibit an oxidation pathway producing MO^+, where M stands for a transition metal,[7] but late transition metals such as Fe^+, Co^+, and Ni^+ (including Cr^+) participate in decarbonylation reactions producing MCO^+.[5,6,8] Because of the strong metal−oxo bond of the early transition metals, the reactions of these bare metals (Ti^+ and Sc^+) with acetaldehyde lead to the oxidation of metal ions.[22,23] The reaction of metal cations with acetone, which is more complex than with acetaldehyde, is expected to show a similar trend. It has been shown that Fe^+, Co^+, and Ni^+ react readily with acetone to give MCO^+ and CH_3-CH_3 as products.[24,25] The decarbonylation process by these late transition metals proceeds through three elementary steps: oxidative insertion of the metal ion into the C−C bond of acetone, methyl-group migration, and reductive elimination. On the other hand, owing to the extremely strong binding of the metal ions to oxygen atom, the reaction of acetone with Sc^+, Ti^+, Gd^+, and Pr^+ only undergoes oxidation of the metal ions, which gives completely different products (MO^+ and C_3H_6).[22,23,26] Recently, density functional theory (DFT) has been employed to investigate the decarbonylation of acetone with Ni^+.[16] This theoretical study not only rationalizes experimental findings but also gives a deeper insight to the reaction mechanism. However, there have not been similar theoretical studies on the reaction of an early transition-metal ion such as Sc^+ and Ti^+ with acetone. To have a comprehensive understanding of the reaction of a transition-metal ion with acetone, it is logical to extend theoretical investigations to the early transition-metal ions.

In the present work, the reaction of Ti^+ with acetone is investigated by using the DFT[27,28] and ab initio methods. Because the reaction of Ti^+ with acetone is spin-forbidden, the spin-orbit (SO) effect is expected to play a key role in the reaction mechanism.[29,30] Although the SO effect plays an important role in potential-energy surfaces (PESs) including open-shell transition metals, it has often been neglected because of the computational complexity involved. In this work, the intersystem crossing (ISC) point is optimized by using a multireference ab initio method, and the SO effect near the ISC point is examined. Thus, by using the systematic computational approach, we fully investigate the reaction of Ti^+ with a specific organic molecule.

Computational Details

The molecular geometries and harmonic vibrational frequencies were calculated by using DFT. The PBE0[31,32] (Hybrid, 25% of the exact exchange energy) functional was used for the reaction of Ti^+ with acetone. All geometry optimizations were

* Corresponding authors. E-mail: hyotcherl.ihee@kaist.ac.kr (H. I.) and tkkim@pusan.ac.kr (T. K. K.).
[†] Graduate School of Nanoscience & Technology (WCU).
[‡] Pusan National University.

10.1021/jp905158j CCC: $40.75
Published on Web 09/28/2009

performed without symmetry constraints. The aug-cc-pVTZ basis sets were used for Ti (Ti, [8s7p5d3f2g])[33] and other atoms (C and O, [5s4p3d2f]; H, [4s3p2d]). In addition, the aug-cc-pVQZ basis sets (Ti, [9s8p6d4f3g2h]; C and O, [6s5p4d3f2g]; H- [5s4p3d2f]) were used for the single-point calculations to examine basis-set dependence. The coupled-cluster singles and doubles method including a perturbative estimate of triples (CCSD(T))[34] was used to compare relative energies calculated by the DFT method. Because the size of Ti^+-acetone complex is too large for the calculation at the CCSD(T)/aug-cc-pVTZ level, we reduced the size of basis sets by excluding the diffuse function. In this regard, the CCSD(T)/cc-pVTZ (Ti, [7s6p4d2f1g];[33] C and O, [4s3p2d1f]; H, [3s2p1d]) was used for the single-point calculations. The reaction energy ($^4Ti^+ + CH_3COCH_3 \rightarrow {}^2TiO^+ + CH_2CHCH_3$) calculated by the CCSD(T)/cc-pVTZ (−35.6 kcal/mol) was in good agreement with that of the CCSD(T)/aug-cc-pVTZ (−34.2 kcal/mol). Thus, we safely used the CCSD(T)/cc-pVTZ for the single-point calculations. All single-point calculations were performed at the geometries optimized by the PBE0/aug-cc-pVTZ level, and all energies were reported with the zero-point energy (ZPE) corrections. The ZPE values of the PBE0/aug-cc-pVTZ level were used for the corrections. All transition states presented in this work were identified by one imaginary frequency and confirmed by using the intrinsic reaction coordinate (IRC) method.[35,36] We also used the natural population analysis (NPA)[37] for characterizing atomic charges and electronic structures. All calculations were performed by using the Gaussian03 program.[38]

The complete active space SCF (CASSCF) method[39] was used to optimize the ISC point. Eleven electrons were distributed in the 11 active orbitals (CAS(11,11)), and the scalar relativistic effect was considered by using the Douglas−Kroll−Hess second-order method (DKH2).[40,41] The active space involved five d, one s, and three p orbitals of Ti and π and π^* orbitals of C═O (total 11 orbitals). The SO effect near the ISC point was considered by using the RASSI-SO method[42] at both CASSCF and CASPT2 (multiconfigurational second-order perturbation theory)[43,44] levels. In the CASSCF and CASPT2 calculations, the ANO-RCC basis sets[45] were used for all elements (Ti, (21s15p10d6f)/[6s5p3d2f]; C, (14s9p4d)/[3s2p1d]; O, (14s9p4d)/[3s2p1d]; and H, (8s4p)/[2s1p]). All multireference ab initio calculations were performed by using the Molcas6.4 program.[46]

For the optimization of the crossing point between doublet and quartet states, we optimized both spin states simultaneously with the constraint that the energy difference between the two states is equal to zero. Then, we optimized the minimum energy crossing point (MECP) between doublet and quartet PESs.[29] and the ISC took place at the MECP. This method has been previously applied to simple organic reactions.[47,48] The optimization of the MECP was performed by using the SLAPAF program in the Molcas6.4. We only used the CASSCF method to optimize the crossing point because of by the deficiency of analytical gradient of the CASPT2 method. However, the CASPT2 energies were calculated by using the CASSCF optimized geometries to consider the dynamic electron correlation effect.

To calculate the transition probability from quartet state to doublet state at the MECP, we used the Landau−Zener formula.[49] The Landau−Zener transition probability ($P(i,j)$) between two adiabatic states i and j is given by

$$P(i,j) = 1 - e^{-2\delta_{ij}}, \delta_{ij} = \pi \frac{|V_{ij}|}{\hbar v |g_i - g_j|} = \pi \frac{C_{S,S'}}{(2\min(S_i, S_j))\hbar v |g_i - g_j|}$$

$$(\mathrm{SOCC})^2 = C_{S,S'} \equiv \sum_{M_S=-S}^{S} \sum_{M_{S'}=-S'}^{S'} |\langle SM_S|\hat{H}_{SO}|S'M_{S'}\rangle|^2$$

where g is the adiabatic energy gradient, v is the effective velocity at the transition point that can be calculated from the kinetic theory of gases at 298 K, and V_{ij} is a matrix element of a SO operator. The SOCC term represents the SO coupling constant.

Results and Discussion

In the following subsections, the reactants and products of the reaction between Ti^+ and acetone are discussed, and theoretical results are presented for three plausible reaction pathways: (1) direct metal-ion insertion into the C═O bond, (2) direct H shift, and (3) metal-mediated H migration. The ISC induced by the SO coupling is discussed after the subsection describing the direct metal-ion insertion into the C═O bond. $^4Ti^+$ (the superscript denotes the spin multiplicity) with CH_3COCH_3 (acetone) was used for the reference energy on all reaction PESs. That is, all energy values are relative to the reference energy.

Reactants and Products. To select an appropriate DFT functional, we calculated the bond dissociation energies (BDE) of $Ti^+(H_2O)_n$, $Ti^+(NH_3)_n$, and $Ti^+(C_2H_4)$. The calculated results are summarized in Table S1 in the Supporting Information. The BDEs calculated by the PBE0 are in excellent agreement with the experiments, and thus, we selected the PBE0 functional for the calculation of reaction of Ti^+ with acetone.

Optimized geometrical parameters of the reactants (CH_3COCH_3 (acetone)) and products (TiO^+, CH_2CHCH_3 (propene) and C_3H_6 (cyclopropane)) are shown in Figure 1. The PBE0 predicts that the doublet of TiO^+ ($^2TiO^+$, $^2\Delta$) is more stable than the quartet ($^4TiO^+$, $^4\Delta$), and the energy difference between $^2TiO^+$ and $^4TiO^+$ is 71.1 kcal/mol (71.2 kcal/mol at the aug-cc-pVQZ level), which reasonably agrees with the value obtained by the CCSD(T)/aug-cc-pVTZ (77.5 kcal/mol). Among two isomers of C_3H_6 (cyclopropane and propene), cyclopropane lies 5.0 kcal/mol (4.8 kcal/mol at the aug-cc-pVQZ level) higher in energy than CH_2CHCH_3 (propene). Thus, we considered the channels leading to CH_2CHCH_3 as the major product.

Direct Metal-Ion Insertion into the C═O Bond. All optimized structures and the relevant PES along with the pathway of direct metal-ion insertion into the C═O bond are depicted in Figures 1 and 2, respectively, and all relative energies are summarized in Table 1. In this paper, we used the notations of IMn and TS$n-m$ for the intermediate n and the transition state between the IMn and the IMm, respectively. The superscript in the notations denotes the spin multiplicity.

Initially, a Ti^+ ion attacks the electron-rich oxygen of the acetone and forms stable intermediate structures (^{2}IM1 and ^{4}IM1), where the Ti−O−C angle is 180.0°. The structure of this intermediate between Ti^+ and acetone is remarkably different from the bent geometry of Ni^+−acetone complex (Ni^+−O−C: 138.8°), which mainly produces $NiCO^+ + C_2H_6$ products.[16] The ISC occurs between ^{4}IM1 and ^{2}IM2, which we will discuss in detail in the next section. The ^{2}IM2 structure is

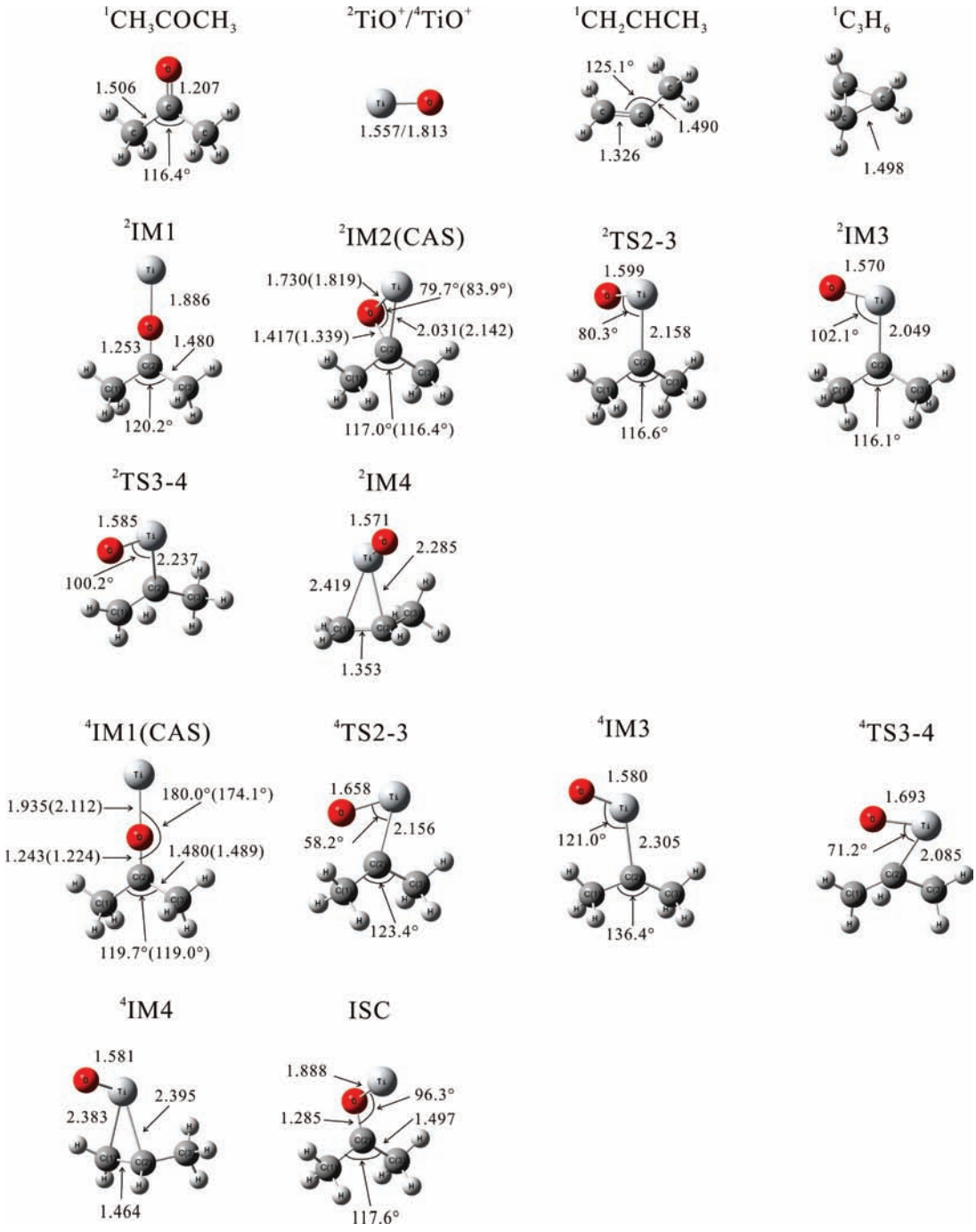

Figure 1. Selected parameters (bond lengths in Å and angles in degree) of optimized geometries of the reactants (Ti^+ and CH_3COCH_3), the products (TiO^+, CH_2CHCH_3 and C_3H_6), the transition states, and the intermediates calculated by the PBE0/aug-cc-pVTZ on reaction PESs of the direct metal-ion insertion into the C═O bond pathway. Values in parentheses were calculated by the CAS(11,11). The ISC point was optimized by using the CAS(11,11). The superscript denotes the spin multiplicity.

characterized by a three-membered ring of Ti—O—C and Ti^+ directly coordinated with the C(2) atom. The C(2)—O bond is weakened and substantially elongated in both ^{2}TS2−3 and ^{4}TS2−3 compared with ^{2}IM2 (see Figure 1). In both ^{2}IM3 and ^{4}IM3, the Ti atom is located between the C and O atoms, and both the Ti—O bond and the C—C bonds lie in the same plane according to the dihedral angle of CCTiO. As can be seen in both ^{2}IM3 and ^{4}IM3, Ti^+ is effectively inserted into the C═O bond along this reaction pathway. The H atom then migrates to the C(2) atom, forming ^{2}IM4 and ^{4}IM4 structures. The ^{2}IM4 is the final intermediate structure on the doublet PES in all other reaction pathways (see other sections).

The atomic charge of Ti calculated by the NPA in the ^{4}IM1 is close to the one. In other words, Ti in ^{4}IM1 has the character of a bare Ti^+ atom. However, as shown in Table 1, the Ti and C(2) of ^{2}IM2 have considerably different atomic charges compared with those of ^{4}IM1, with increased positive charge in Ti and reduced positive charge in C(2). Thus, we expect that electrons move from Ti to C(2) through the reaction proceeding from the ^{4}IM1 to the ^{2}IM2. To clarify this issue, we depict relevant molecular orbitals (MOs) and summarize natural electron configurations of ^{4}IM1 and ^{2}IM2 in Figure S1 in the Supporting Information. One unpaired α electron in a quartet state has to be converted into a β electron to become a doublet.

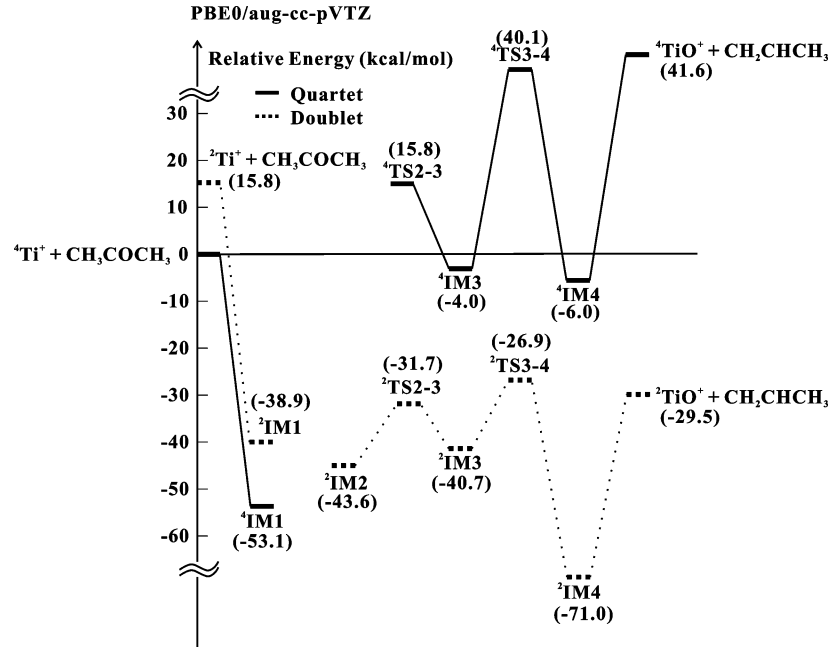

Figure 2. Reaction PESs of the direct metal-ion insertion into the C═O bond pathway at the PBE0/aug-cc-pVTZ level. The related optimized structures are depicted in Figure 1, and their energies are summarized in Table 1.

TABLE 1: Relative Energies (ΔE, kcal/mol) Calculated by the PBE0/aug-cc-pVTZ, Single-Point Relative Energies ($\Delta E_{CCSD(T)}$, kcal/mol) Calculated by the CCSD(T)/cc-pVTZ, Atomic Charges (NPA), and $\langle S^2 \rangle$ Values for all Species Involved in the Direct Metal-Ion Insertion into the C═O Bond Pathway[a]

		Doublet							
		$^2Ti^+ + CH_3COCH_3$	$^2IM1$	$^2IM2$	$^2TS2-3$	$^2IM3$	$^2TS3-4$	$^2IM4$	$^2TiO^+ + CH_2CHCH_3$
ΔE		15.8(15.7)	−38.9(−39.0)	−43.6(−43.3)	−31.7(−31.3)	−40.7(−40.2)	−26.9(−26.5)	−71.0(−70.5)	−29.5(−29.2)
$\Delta E_{CCSD(T)}$		4.1, *4.1*[e]	−38.9	−39.8	−30.4	−36.8	−26.8	−71.7	−35.6, *−34.2*[e]
[b]Atomic Charges	Ti	1.000	0.978	1.497	1.406	1.493	1.444	1.365	1.607
	O	−0.539	−0.745	−0.614	−0.621	−0.568	−0.661	−0.545	−0.607
	C(1)	−0.714	−0.711	−0.665	−0.741	−0.718	−0.192	−0.455	−0.406
	C(2)	0.584	0.633	0.033	0.085	−0.062	−0.506	−0.218	−0.169
	C(3)	−0.714	−0.711	−0.665	−0.748	−0.731	−0.655	−0.685	−0.643
$\langle S^2 \rangle$		1.751[c]	1.757	0.777	0.759	0.756	0.759	0.758	0.761[d]

		Quartet						
		$^4Ti^+ + CH_3COCH_3$	$^4IM1$	$^4TS2-3$	$^4IM3$	$^4TS3-4$	$^4IM4$	$^4TiO^+ + CH_2CHCH_3$
ΔE		0.0(0.0)	−53.1(−53.1)	15.8(16.4)	−4.0(−3.5)	40.1(40.6)	−6.0(−5.5)	41.6(42.0)
$\Delta E_{CCSD(T)}$		0.0	−47.4	26.8	0.1	59.2	−1.9	42.3, *43.3*[e]
[b]Atomic Charges	Ti	1.000	0.921	1.294	1.532	1.131	1.328	1.470
	O	−0.539	−0.738	0.596	−0.689	−0.558	−0.605	−0.470
	C(1)	−0.714	−0.717	−0.736	−0.770	−0.282	−0.358	−0.406
	C(2)	0.584	0.674	0.184	0.039	−0.282	−0.206	−0.169
	C(3)	−0.714	−0.717	−0.727	−0.757	−0.655	−0.694	−0.643
$\langle S^2 \rangle$		3.751[c]	3.755	3.767	3.765	3.766	3.765	3.753[d]

[a] Values in parentheses are calculated by the aug-cc-pVQZ. [b] The related figures are depicted in Figure 1. [c] This value is the $\langle S^2 \rangle$ value of Ti^+. CH_3COCH_3 is the singlet state. [d] This value is the $\langle S^2 \rangle$ value of TiO^+. CH_2CHCH_3 is the singlet state. [e] The single-point energy calculated by the CCSD(T)/aug-cc-pVTZ.

As shown in Figure S1, an unpaired α electron in the 4*s* orbital of Ti is converted into a β electron in the MO the shape of which is a mixture of a d orbital of Ti and a p orbital of C(2) in the ^{4}IM1. This spin flip can be confirmed by the change in the natural electron configuration. First, the occupation number of α 4s in Ti is reduced from 0.66 to 0.10 as the reaction proceeds from the ^{4}IM1 to ^{2}IM2. In contrast, the occupation number of β 3d in Ti increases from 0.06 to 0.61, whereas that of β 2p in C(2) increases from 1.15 to 1.51. These results are consistent with the MO analysis. However, we note that the occupation number of α 3d in Ti, which is not directly involved in this argument, decreases from 2.33 to 1.72 instead of staying constant. This change might mean that the charge of α 3d in Ti is also transferred to the C(2) atom as the interaction between Ti and C(2) increases by the transition from the ^{4}IM1 to ^{2}IM2. In summary, as the reaction proceeds from the ^{4}IM1 to ^{2}IM2 with the Ti—O—C angle being bent, α electron of 4s orbital in Ti is transferred to β electron of 3d in Ti and 2p in C(2). Such a spin-flipping process is governed by the SO coupling that induces the ISC. Details of the ISC are treated in the following subsection.

As has been mentioned above, the ^{2}IM4 is the final intermediate in all reaction pathways. In its structure, two carbon atoms of CH_2CHCH_3 are weakly coordinated to $^2TiO^+$, as can be verified by large bond distances between Ti and C's (see Figure 1). Such coordination in the ^{2}IM4 structure can be confirmed by the C═C bond of CH_2CHCH_3 unit in the ^{2}IM4. The geometry parameters of the CH_2CHCH_3 unit in the ^{2}IM4 is

similar to those of propene, except that the C═C bond distance of ^{2}IM4 (1.353 Å) is larger than that of propene (1.326 Å). The larger C═C bond distance indicates that the 3d orbital of Ti interacts with π^* orbital of C═C bond (see singly occupied molecular orbital (SOMO) of the ^{2}IM4 in Figure S2 in the Supporting Information).

The reaction energy of the $^4Ti^+ + CH_3COCH_3 \rightarrow {}^2TiO^+ + CH_2CHCH_3$ reaction is calculated to be −29.5 (−29.2) kcal/mol at the PBE0/aug-cc-pVTZ (aug-cc-pVQZ) level. As the size of basis set increases, the reaction energy slightly changes. This trend universally applies to all molecular structures reported in this study, and the variation of reaction energy depending on the basis set is generally about 0.2−0.6 kcal/mol. Although the PBE0/aug-cc-pVTZ (−29.5 kcal/mol) slightly underestimates the reaction energy compared with the CCSD(T)/aug-cc-pVTZ (−34.2 kcal/mol), it still gives relative energies that are very close to those calculated by the CCSD(T)/aug-cc-pVTZ, except for some cases (^{4}TS2−3 and ^{4}TS3−4). Thus, we conclude that the PBE0/aug-cc-pVTZ level can calculate the thermochemical energy in a cost-effective manner.

The barrier height between the ^{2}IM3 and ^{2}TS3−4 (PBE0: 13.8 and CCSD(T): 10.0 kcal/mol) is the largest on the doublet PES of this pathway, but this value is still the smallest among the largest barrier height in other pathways (see other section). This result indicates that this pathway is likely the most energetically favorable reaction pathway.

As mentioned above, the results of the PBE0 are quite consistent with those of the CCSD(T), except for the ^{4}TS2−3 and the ^{4}TS3−4. This finding may be related to the well-known tendency that the barrier heights are underestimated in the calculations using the hybrid DFT methods. For example, when using the PBE0, the barrier height between the ^{4}IM3 and the ^{4}TS3−4 is calculated to be 44.1 kcal/mol, which is an underestimated value compared with 59.1 kcal/mol calculated by the CCSD(T). This underestimation of barrier height is attributed to overstabilization of the transition states by the PBE0. This tendency is large on quartet PES, whereas it is negligible on doublet. The same tendency applies to other reaction pathways (see other section).

ISC. Although there exist other ISC points, here, we focus on the ISC point between ^{4}IM1 and ^{2}IM2, because this ISC point is directly related to the most favorable reaction pathway of the direct metal-ion insertion. Despite many efforts aimed at finding the transition state between IM1 and IM2 on both doublet and quartet states, neither TS1−2 on the doublet and quartet states nor ^{4}IM2 in the quartet state have been identified. Thus, we assumed that there is an ISC between ^{4}IM1 and ^{2}IM2. A schematic representation of this assumption is depicted in Figure 3a. The CAS(11,11) method was employed to find the ISC point (i.e., MECP). As shown in Figure 1, the main difference between ^{4}IM1 and ^{2}IM2 is the angle of Ti—O—C (180.0° vs 79.7°). Therefore, we performed single-point energy calculations for both doublet and quartet states by using the CAS(11,11) method while changing the Ti—O—C angle from 180.0 to 90.0°. We checked that the energy difference between the doublet and quartet is sufficiently close to zero and then performed the optimization of the MECP. The result of the optimized geometry of the ISC is depicted in Figure 1. Then, the IRC calculations were performed on the ISC geometry, and then, the quartet and the doublet state converge to the ^{4}IM1 and ^{2}IM2 structures, respectively. The optimized geometries of the ^{4}IM1 and the ^{2}IM2 at the CAS(11,11) level are depicted in Figure 1. The calculated ISC structure indicates that the Ti—O—C angle of the ISC (96.3°) has a value lying between

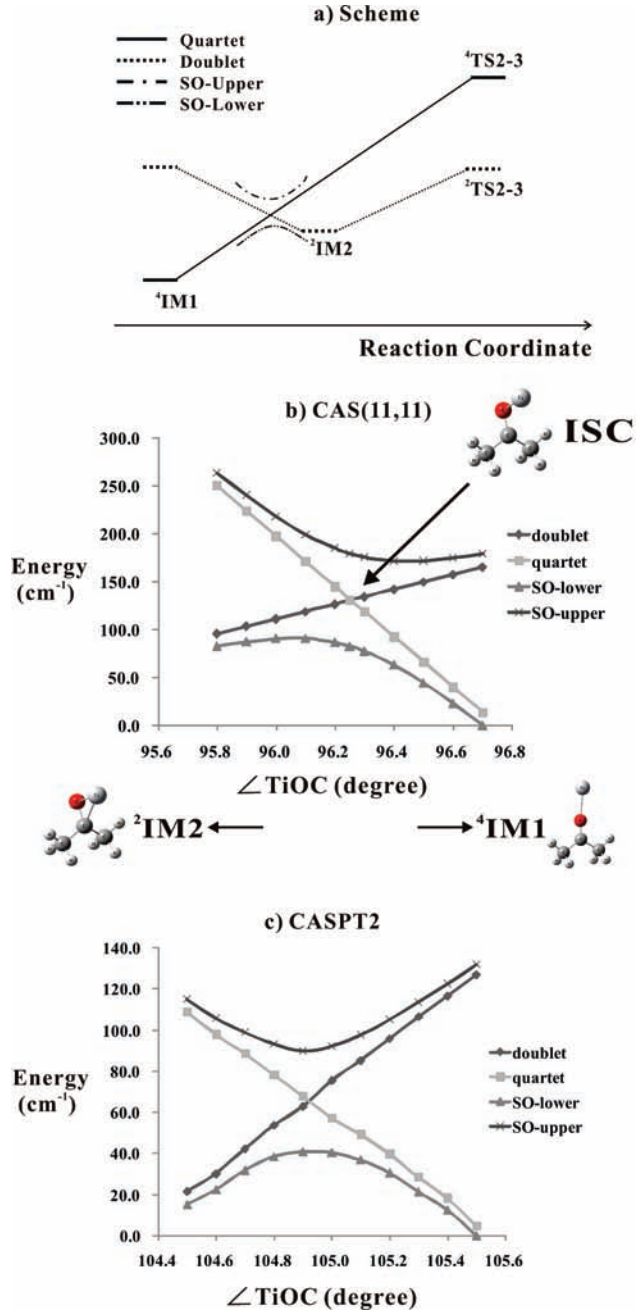

Figure 3. (a) Schematic representation of the reaction PESs near the ISC point. (b) Single-point energy scan along the angle of Ti—O—C at the CAS(11,11) level. (c) Single-point energy scan along the angle of Ti—O—C at the CASPT2 level.

^{4}IM1 (174.1°) and ^{2}IM2 (83.9°). These results confirm that our assumption for the presence of ISC is reasonable, and the bending coordinate of the Ti—O—C is strongly correlated with the reaction coordinate. The energy difference between ^{4}IM1 and ^{2}IM2 calculated by the CAS(11,11) is 35.1 kcal/mol, which is much larger than the values calculated by the PBE0 (9.5 kcal/mol) and the CCSD(T) (7.6 kcal/mol). In contrast, the single-point CASPT2 calculations give 5.7 kcal/mol, which is close to the values from the PBE0 and CCSD(T) calculations. This comparison shows that the CASSCF method is only appropriate for qualitative prediction, and the dynamic correlation effect is still important in order to obtain accurate energy in organometallic complex systems.

The doublet and quartet states on the ISC interact with each other and generate three states: SO-lower, middle, and SO-upper

states. The middle state contains only a pure quartet state, and thus, its energy is the same as that of the quartet state.[9] As mentioned above, the major difference between the ^{4}IM1 and ^{2}IM2 structures is in the Ti—O—C angle (see Figure 1). With the effects of other coordinates being assumed to be negligible, single-point calculations were performed by varying the angle of the Ti—O—C of the ISC geometry from a large angle (^{4}IM1) to a small angle (^{2}IM2). The energies obtained from CAS(11,11) and CASPT2 calculations are plotted in Figure 3b and c, respectively. As shown in Figure 3, the reactants initially produce the ^{4}IM1 structure, and the reaction subsequently proceeds to the ^{2}IM2 along the adiabatic SO-lower PES. The magnitude of the SO splitting (the energy difference between the SO-upper and the SO-lower state) at the ISC geometry is 96.8 cm^{-1} at the CAS(11,11) level of theory. This value is similar to the one obtained from a previous study on the reaction of Ti^+ with ethane.[9] Because the single-point calculations were based on the optimized geometry calculated by the CAS(11,11), the result of the CASPT2 does not yield a smooth curve but clearly shows the same trend as the CAS(11,11) result. Because the effects of other coordinates are neglected here, each method produces slightly different Ti—O—C angles for the ISC (CAS(11,11), 96.3° and CASPT2, near 104.9°). Therefore, it is evident that the dynamic correlation also affects the location of the ISC.

The Landau—Zener transition probability from quartet state to doublet state at the ISC point is 6.1%, which is relatively small compared with those for the reactions of Ti^+ with ethane[9] and methanol.[21] However, the SOCC value (68.4 cm^{-1}) is larger than those of the previous two studies. The small transition probability is attributed to the large value of the difference of gradient ($|g_i - g_j|$, see the Landau—Zener formula in the Computational Details section) calculated by the CASSCF. As mentioned above, because the CASSCF is only good for qualitative prediction, the probability calculated by using the CASSCF results might not be accurate. Therefore, we expect that the actual transition probability is larger than 6.1%. In addition, even if the transition probability is small, it is unlikely that the reaction proceeds on the quartet PES, because the barrier height between ^{4}IM1 and ^{4}TS2—3 is too high (PBE0, 68.9 and CCSD(T), 74.2 kcal/mol). Therefore, we conclude that the reaction predominantly occurs on the doublet PES for direct metal-ion insertion pathway.

Direct H Shift. All optimized structures and the reaction PESs in the direct H-shift pathway are depicted in Figures S3 and S4 in the Supporting Information, respectively, (^{2}IM1 and ^{4}IM1 that have been already discussed in the direct metal-ion insertion channel in the preceding subsection also appear in this pathway and thus are depicted in Figure 1), and all relative energies are summarized in Table S2 in the Supporting Information (^{2}IM1 and ^{4}IM1 are summarized in Table 1). Through both ^{2}TS1—5 and ^{4}TS1—5, the H is migrated from the methyl group to the C(2), leading to the formation of ^{2}IM5 and ^{4}IM5. The Ti—O—C moiety is bent in both ^{2}TS5—6 and ^{4}TS5—6 structures. On the quartet state, the ^{4}IM6 is formed before proceeding to ^{4}IM7, but, on the doublet state, the ^{2}IM7 is directly formed without any intermediate. The doublet state lies lower in energy than the quartet state after ^{2}TS5—6 and ^{4}TS5—6 structures. Thus, the crossing point may be located between ^{4}TS5—6 and ^{4}IM6. The ^{4}TS5—6 is similar in its structure to ^{2}TS5—6, and the Ti—O—C angle of the ^{4}IM6 is more bent than that of the ^{4}TS5—6. When the Ti—O—C angle is reduced, the energy of doublet state is lowered compared with the quartet state and then passes through the ISC, leading to the formation of ^{2}IM7. The Ti—O—C bending coordinate may be related to the ISC point, like in the pathway of direct metal-ion insertion into the C═O bond. Thus, it is clear that an ISC point is expected to be located between ^{4}TS5—6 and ^{4}IM6. After passing this ISC point, the reaction proceeds to the products on the doublet PES. The C—O bond is elongated in both the ^{4}TS6—7 and ^{4}TS6—8 structures, leading to ^{4}IM7 and ^{4}IM8, respectively. The Ti atom is weakly and temporarily coordinated with two C atoms of the ^{2}IM7 and ^{2}IM4 (^{4}IM7 and ^{4}IM8 on the quartet), which then dissociate into the TiO^+ and CH_2CHCH_3 as final products. However, ^{2}IM1, ^{2}TS1—5, ^{2}IM5, ^{2}TS5—6, and $^2Ti^+$ on doublet PES are highly spin-contaminated (see Table 1 and Table S2 in the Supporting Information). Therefore, a multireference-based method and, subsequently, a method treating the SO effect are needed to clearly resolve the PES of this reaction.

The relative energies calculated by the CCSD(T) are reasonably close to those of the PBE0 except for some cases like in the pathway of direct metal-ion insertion into the C═O bond. The discrepancies between PBE0 and CCSD(T) on quartet are generally larger than on doublet. Especially, the discrepancies of the transition states are larger than those of the intermediates. The barrier height between IM1 and TS1—5 on both doublet (46.3 kcal/mol) and quartet (51.0 kcal/mol) are larger than other activation barrier height in this reaction pathway. Hence, the hydrogen-transfer step requires large activation energy as the direct metal-ion insertion into the C═O bond pathway. The barrier heights calculated by the PBE0 are similar to those of CCSD(T) except for the barrier height between IM1 and TS1—5 on both doublet and quartet. The PBE0 underestimates this barrier height (doublet, 46.3 and quartet, 51.0 kcal/mol) compared with the CCSD(T) (doublet, 55.7 and quartet, 60.3 kcal/mol).

Metal-Mediated H Migration. All optimized structures and the reaction PES in the metal-mediated H migration pathway are depicted in Figures S5 and S6 in the Supporting Information, respectively (^{2}IM1, ^{4}IM1, and ^{2}IM2 that have been already discussed in the direct metal-ion insertion channel in the preceding subsection also appear in this pathway and thus are depicted in Figure 1), and all relative energies are summarized in Table S3 in the Supporting Information (^{2}IM1, ^{4}IM1, and ^{2}IM2 are summarized in Table 1). The metal-mediated H migration pathway starts from ^{4}IM1, passes through the ISC, and subsequently ^{2}IM2 is formed, as in the pathway of the direct metal-ion insertion into the C═O bond. Ti attracts one of the H atoms in the methyl group, and the five-membered ring structures of the IM9 are formed on both doublet and quartet PESs. It should be noted that the PBE0 predicts that ^{4}TS2—9 is more stable than ^{2}TS2—9, but the CCSD(T) gives the opposite result (see Table S3 in the Supporting Information). In this case, the PBE0 provides the wrong energy ordering, whereas the CCSD(T) gives the correct one. The structure of the ^{2}IM9 is different from that of the ^{4}IM9. The H atom is already ruptured from the methyl group and coordinated with Ti in the ^{2}IM9, whereas the H atom is still coordinated to the methyl group in the ^{4}IM9. The H atom is ruptured through the ^{4}TS9—10', and thus, the bond distance of Ti—H (2.369 Å) is quite large in the ^{4}IM10' structure. The PBE0 predicts that the barrier height between ^{2}IM2 and ^{2}TS2—9 (5.7 kcal/mol) is small, but that the one between ^{4}IM9 and ^{4}TS9—10' (39.0 kcal/mol) is large. Thus, it is suggested that the H atom is easily detached by the Ti atom on the doublet PES but not on the quartet PES.

As shown Figures S5 and S6 in the Supporting Information, the ^{2}IM9 proceeds via the ^{2}TS9—10 structure to the ^{2}IM10

structure on the doublet PES. In contrast, on the quartet PES, the transition from ^{4}IM9 to ^{4}IM10 occurs in two steps involving an extra intermediate (^{4}IM10') and thus two transition states (^{4}TS9−10' and ^{4}TS10'−10). In the TS10−11 states on both PESs, Ti is coordinated with the H atom, and the H atom is being transferred from the Ti to the O atom. After TS10−11, the H atom is associated with the O atom in IM11 on both PESs. Through TS11−12, the C(2)—O bond is broken, and the Ti atom is coordinated with only the C(2) atom in IM12. A four-membered ring structure is assembled, and the H atom migrates from the O atom to the central C(2) atom in both ^{2}TS12−4 and ^{4}TS12−8. Finally, the ^{2}IM4 and ^{4}IM8 structures are formed on both PESs. In summary, the Ti atom acts as the carrier of the H atom in the metal-mediated H migration pathway.

As shown in Figure S6 in the Supporting Information, ^{2}TS10−11 and ^{2}IM11 states lie higher in energy than their counterparts in the quartet states. The CCSD(T) also gives the same energy ordering (see Table S3 in the Supporting Information). The reversal of energy ordering between doublet and quartet means that ISCs can possibly exist near this region of the PESs. However, we do not expect the presence of any ISC near ^{2}TS10−11 and ^{2}IM11 states, because these states are not related to the bending coordinate of the Ti—O-C. In addition, these doublet states are spin-contaminated (see Table S3 in the Supporting Information) so that the PBE0 and even CCSD(T) cannot provide accurate energies. For these reasons, in reality, these doublet states may lie below their quartet counterparts. Therefore, we conclude that, after the ISC between ^{4}IM1 and ^{2}IM2, the reaction in this pathway proceeds to the products through each of the two adiabatic PESs without any crossing.

The discrepancies between the relative energies calculated by the PBE0 and CCSD(T) are generally small, but, in some cases, they reach or even exceed 10 kcal/mol. However, both methods give the same trend of energy ordering except for the ^{2}TS2−9. The barrier height between ^{2}IM10 and ^{2}TS10−11, which is the hydrogen-transfer process, is the largest, as in the other two pathways. In contrast, on the quartet PES, the detachment of H from methyl group requires large activation energy. All barrier heights on quartet PES, except for the one between ^{4}IM9 and ^{4}TS9−10', are slightly underestimated by the PBE0 compared with those calculated by the CCSD(T).

Most Favorable Reaction Pathway. The pathway of direct metal-ion insertion into the C═O bond is simple and has a lower activation energy than that of other reaction pathways. Therefore, the direct metal-ion insertion into the C═O bond reaction pathway is likely to be the most favorable pathway for the oxidation process of Ti^+, like for the reaction between Ti^+ and acetaldehyde.[7] On the basis of the above results, we propose the most favorable reaction pathway as follows:

$$^4Ti^+ + CH_3COCH_3 \rightarrow {}^4IM1 \rightarrow ISC \rightarrow {}^2IM2 \rightarrow {}^2TS2-3 \rightarrow {}^2IM3 \rightarrow {}^2TS3-4 \rightarrow {}^2IM4 \rightarrow {}^2TiO^+ + CH_2CHCH_3$$

Through this reaction pathway, Ti^+ is most efficiently oxidized by acetone (CH_3COCH_3).

Brief Comment on C—H Activation. We also examined the C—H activation channel by Ti^+, which is initiated by the insertion of the metal ion into the C—H bond, but we could not find the transition state on either doublet or quartet PESs. However, we found the intermediate structures ($^2IM_{C-H}$ and $^4IM_{C-H}$), which are expected to be the first intermediates on the C—H activation coordinate. The molecular structures of these intermediates are depicted in Figure S7, and the relative energies are summarized in Figure S8 in the Supporting Information. The $^2IM_{C-H}$ and $^4IM_{C-H}$ lie 54.6 and 38.6 kcal/mol higher in energy than the ^{4}IM1, respectively. The $^4IM_{C-H}$ lie even 12.4 kcal/mol higher in energy than ^{2}TS3−4, which is located at the highest energy point of the doublet surface in the pathway of the direct metal-ion insertion into the C═O bond. Thus, we conclude that the C—H activation coordinate is much higher in energy than other oxidation pathways, and thus, this reaction pathway is not favorable in terms of energetics.

Conclusions

Three reaction pathways of Ti^+ with CH_3COCH_3 have been investigated by using DFT and ab initio methods: (1) direct metal-ion insertion into the C═O bond, (2) direct H shift, and (3) metal-mediated H migration. These reaction pathways account for how Ti^+ activates the C═O bond in CH_3COCH_3 and is subsequently oxidized. The PBE0 functional gives good results that are reasonably close to those obtained by the CCSD(T).

In this work, an ISC point is identified, and the SO effect is examined near the ISC point by using a multireference ab initio method. The CASSCF and CASPT2 methods produce similar trends for the adiabatic SO PESs, but the locations of the ISC are slightly different between the two methods. The dynamic electron correlation considerably affects the PES of the reaction, and the CASSCF gives only qualitatively acceptable results. On the basis of the calculation results, it is suggested that the bending coordinate of the Ti—O—C angle is strongly correlated with the ISC. Our theoretical results clearly show that the most favorable reaction pathway passing the ISC is the pathway of direct metal-ion insertion into the C═O bond.

Acknowledgment. We appreciate the help of Jeongho Kim. This work was supported by the Creative Research Initiatives (Center for Time-Resolved Diffraction) of MEST/NRF.

Supporting Information Available: Bond dissociation energies of $Ti^+(H_2O)_n$, $Ti^+(NH_3)_n$, and $Ti^+(C_2H_4)$ are also summarized in Table S1. Molecular orbitals of ^{4}IM1, ^{2}IM2, and ^{2}IM4 are depicted in Figures S1 and S2, respectively. Selected parameters of optimized geometries and the reaction potential energy surfaces in the direct H-shift pathway are shown in Figures S3 and S4, respectively. The same parameters in the metal-mediated H migration reaction pathway are also shown in Figures S5 and S6. Relative energies, atomic charges, and $\langle S^2 \rangle$ values for all species involved in the direct H shift and the metal-mediated H migration reaction pathways are summarized in Tables S2 and S3, respectively. The optimized geometries of intermediates on the C—H activation reaction coordinates are shown in Figure S7, and their relative energies are summarized in Figure S8. This material is available free of charge via the Internet at http://pubs.acs.org.

References and Notes

(1) Ritleng, V.; Sirlin, C.; Pfeffer, M. *Chem. Rev.* **2002**, *102*, 1731.
(2) Eller, K.; Schwarz, H. *Chem. Rev.* **1991**, *91*, 1121.
(3) Schröder, D.; Schwarz, H. *Angew. Chem., Int. Ed. Engl.* **1995**, *34*, 1973.
(4) Weisshaar, J. C. *Acc. Chem. Res.* **1993**, *26*, 213.
(5) Chen, X. F.; Guo, W. Y.; Zhao, L. M.; Fu, Q. T.; Ma, Y. *J. Phys. Chem. A* **2007**, *111*, 3566.
(6) Zhao, L. M.; Guo, W. Y.; Zhang, R. R.; Wu, S. J.; Lu, X. Q. *ChemPhysChem* **2006**, *7*, 1345.
(7) Zhao, L. M.; Zhang, R. R.; Guo, W. Y.; Lu, X. Q. *Chem. Phys. Lett.* **2006**, *431*, 56.
(8) Zhao, L. M.; Zhang, R. R.; Guo, W. Y.; Wu, S. J.; Lu, X. Q. *Chem. Phys. Lett.* **2005**, *414*, 28.

(9) Moc, J.; Fedorov, D. G.; Gordon, M. S. *J. Chem. Phys.* **2000**, *112*, 10247.
(10) Moc, J.; Gordon, M. S. *Theor. Chem. Acc.* **2008**, *120*, 243.
(11) Chen, X. X.; Feng, X. S.; Wang, Y. C.; Wang, T.; Liu, X. L.; Zheng, X. W. *Chem. Phys. Lett.* **2007**, *443*, 430.
(12) Wang, Y. C.; Chen, X. X. *Chem. Phys. Lett.* **2006**, *422*, 534.
(13) Zhao, L. M.; Wang, Y.; Guo, W. Y.; Shan, H. H.; Lu, X. Q.; Yang, T. *J. Phys. Chem. A* **2008**, *112*, 5676.
(14) Ding, N.; Zhang, S. G.; Chen, X. X. *Chem. Phys. Lett.* **2008**, *458*, 33.
(15) Wang, Y. C.; Liu, Z. Y.; Geng, Z. Y.; Yang, X. Y. *Chem. Phys. Lett.* **2006**, *427*, 271.
(16) Chen, X. F.; Guo, W. Y.; Zhao, L. M.; Fu, Q. T. *Chem. Phys. Lett.* **2006**, *432*, 27.
(17) Ma, Y.; Guo, W. Y.; Zhao, L. M.; Hu, S. Q.; Zhang, J.; Fu, Q. T.; Chen, X. F. *J. Phys. Chem. A* **2007**, *111*, 6208.
(18) Zhao, L. M.; Guo, W. Y.; Yang, T. F.; Lu, X. Q. *J. Phys. Chem. A* **2008**, *112*, 533.
(19) Lu, X. Q.; Guo, W. Y.; Yang, T. F.; Zhao, L. M.; Du, S. C.; Wang, L.; Shan, H. H. *J. Phys. Chem. A* **2008**, *112*, 5312.
(20) Alcami, M.; Luna, A.; Mo, O.; Yáñez, M.; Tortajada, J. *J. Phys. Chem. A* **2004**, *108*, 8367.
(21) Zhang, F. Y.; Guo, W. Y.; Zhao, L. M.; Lin, X. Q.; Zhang, L. Z.; Zhu, H. Y.; Shan, H. H. *J. Phys. Chem. A* **2009**, *113*, 7103.
(22) Allison, J.; Ridge, D. P. *J. Am. Chem. Soc.* **1978**, *100*, 163.
(23) Tolbert, M. A.; Beauchamp, J. L. *J. Am. Chem. Soc.* **1984**, *106*, 8117.
(24) Burnier, R. C.; Byrd, G. D.; Freiser, B. S. *Anal. Chem.* **1980**, *52*, 1641.
(25) Hanratty, M. A.; Beauchamp, J. L.; Illies, A. J.; van Koppen, P.; Bowers, M. T. *J. Am. Chem. Soc.* **1988**, *110*, 1.
(26) Schilling, J. B.; Beauchamp, J. L. *J. Am. Chem. Soc.* **1988**, *110*, 15.
(27) Hohenberg, P.; Kohn, W. *Phys. Rev. B* **1964**, *136*, 864.
(28) Kohn, W.; Sham, L. J. *Phys. Rev. A* **1965**, *140*, 1133.
(29) Harvey, J. N. *Computational Organometallic Chemistry*; Cundari, T. R., Ed.; Marcel Dekker, Inc.: New York, 2001; p 291.
(30) Schröder, D.; Shaik, S.; Schwarz, H. *Acc. Chem. Res.* **2000**, *33*, 139.
(31) Adamo, C.; Barone, V. *J. Chem. Phys.* **1999**, *110*, 6158.
(32) Ernzerhof, M.; Scuseria, G. E. *J. Chem. Phys.* **1999**, *110*, 5029.
(33) Balabanov, N. B.; Peterson, K. A. *J. Chem. Phys.* **2005**, *123*, 64107.
(34) Raghavachari, K.; Trucks, G. W.; Pople, J. A.; Head-Gordon, M. *Chem. Phys. Lett.* **1989**, *157*, 479.
(35) Gonzalez, C.; Schlegel, H. B. *J. Chem. Phys.* **1989**, *90*, 2154.
(36) Gonzalez, C.; Schlegel, H. B. *J. Phys. Chem.* **1990**, *94*, 5523.
(37) Reed, A. E.; Curtiss, L. A.; Weinhold, F. *Chem. Rev.* **1988**, *88*, 899.
(38) Frisch, M. J., Trucks, G. W.; Schlegel, H. B.; Scuseria, G. E.; Robb, M. A.; Cheeseman, J. R.; Montgomery, Jr., J. A.; Vreven, T.; Kudin, K. N.; Burant, J. C.; Millam, J. M.; Iyengar, S. S.; Tomasi, J.; Barone, V.; Mennucci, B.; Cossi, M.; Scalmani, G.; Rega, N.; Petersson, G. A.; Nakatsuji, H.; Hada, M.; Ehara, M.; Toyota, K.; Fukuda, R.; Hasegawa, J.; Ishida, M.; Nakajima, T.; Honda, Y.; Kitao, O.; Nakai, H.; Klene, M.; Li, X.; Knox, J. E.; Hratchian, H. P.; Cross, J. B.; Bakken, V.; Adamo, C.; Jaramillo, J.; Gomperts, R.; Stratmann, R. E.; Yazyev, O.; Austin, A. J.; Cammi, R.; Pomelli, C.; Ochterski, J. W.; Ayala, P. Y.; Morokuma, K.; Voth, G. A.; Salvador, P.; Dannenberg, J. J.; Zakrzewski, V. G.; Dapprich, S.; Daniels, A. D.; Strain, M. C.; Farkas, O.; Malick, D. K.; Rabuck, A. D.; Raghavachari, K.; Foresman, J. B.; Ortiz, J. V.; Cui, Q.; Baboul, A. G.; Clifford, S.; Cioslowski, J.; Stefanov, B. B.; Liu, G.; Liashenko, A.; Piskorz, P.; Komaromi, I.; Martin, R. L.; Fox, D. J.; Keith, T.; Al-Laham, M. A.; Peng, C. Y.; Nanayakkara, A.; Challacombe, M.; Gill, P. M. W.; Johnson, B.; Chen, W.; Wong, M. W.; Gonzalez, C.; and Pople, J. A.; Revision E.01. Gaussian, Inc.; Wallingford CT; 2004.
(39) Roos, B. O. *Advances in Chemical Physics; Ab Initio Methods in Quantum Chemistry II*; John Wiley and Sons: Chichester, England, 1987; p 399.
(40) Hess, B. A. *Phys. Rev. A* **1986**, *33*, 3742.
(41) Jansen, G.; Hess, B. A. *Phys. Rev. A* **1989**, *39*, 6016.
(42) Malmqvist, P. A.; Roos, B. O.; Schimmelpfennig, B. *Chem. Phys. Lett.* **2002**, *357*, 230.
(43) Andersson, K.; Malmqvist, P. A.; Roos, B. O. *J. Chem. Phys.* **1992**, *96*, 1218.
(44) Andersson, K.; Malmqvist, P. A.; Roos, B. O.; Sadlej, A. J.; Wolinski, K. *J. Phys. Chem.* **1990**, *94*, 5483.
(45) Roos, B. O.; Lindh, R.; Malmqvist, P. A.; Veryazov, V.; Widmark, P. O. *J. Phys. Chem. A* **2004**, *108*, 2851.
(46) Karlstrom, G.; Lindh, R.; Malmqvist, P. A.; Roos, B. O.; Ryde, U.; Veryazov, V.; Widmark, P. O.; Cossi, M.; Schimmelpfennig, B.; Neogrady, P.; Seijo, L. *Comput. Mater. Sci.* **2003**, *28*, 222.
(47) Lu, L. L.; Wang, X. F.; Wang, Y. C.; Wang, H. Q. *J. Mol. Struct. (THEOCHEM)* **2006**, *770*, 1.
(48) Lu, L. L.; Wang, X. F.; Yuan, K.; Wang, Y. C.; Wang, H. Q. *J. Mol. Struct. (THEOCHEM)* **2007**, *809*, 73.
(49) Fedorov, D. G.; Koseki, S.; Schmidt, M. W.; Gordon, M. S. *Int. Rev. Phys. Chem.* **2003**, *22*, 551.

JP905158J